Title: Mapping microplastic movement: A phase diagram to predict microplastics modes of transport

**Authors: Hadeel Al-Zawaidah[1*], Merel Kooi[2], Ton Hoitink[1], Bart Vermeulen[1] & Kryss Waldschläger[1]**

[1]: Wageningen University and Research, Hydrology and Environmental Hydraulics Group, Wageningen, The Netherlands

[2]: Wageningen University and Research, Aquatic Ecology and Water Quality Group, 6700 AA Wageningen, The Netherlands

[*]: Corresponding author, Email: hadeel.alzawaidah@wur.nl

**Key words:** microplastics transport, the transport stage, phase diagram, bedload transport, suspension

## Highlights

- The transport stage $U_*/W_s$ can predict microplastics trajectory characteristics
- Microplastics modes of transport can be predicted by the transport stage
- Microplastics density and nominal diameter governed their particle trajectories
- Particles susceptibility to suspension increase as they deviated from perfect spheres
- A phase diagram was developed to predict microplastics modes of transport

## Abstract

Microplastics pose numerous threats to aquatic environments, yet general understanding of the mechanisms governing their transport remains limited. Drawing upon research on natural sediment provides a valuable resource to address this knowledge gap. One key dimensionless number used to describe sediment transport is the transport stage, referring to the ratio between the fluids shear velocity and the particle settling velocity. However, differences in physical properties (e.g., shape, density) raise concerns regarding the applicability of existing sediment transport theories to microplastics. To address this challenge, we employed a physical modelling approach to examine the trajectories of 24 negatively buoyant microplastic particles varying in size, shape and density. Utilizing a 3D particle tracking setup, we captured the movement of the particles in turbulent open channel flow. A total of 720 trajectories where recorded and analysed. The results revealed a strong correlation between the transport stage and the mean forward velocity of the particles, as well as their mean position in the water column. Notably, particle shape emerged as a critical factor influencing particle transport dynamics. Fibres showed a tendency to be transported closer to the water surface while experiencing slower mean forward velocities compared to spheres. The microplastic particles exhibited rolling/sliding, saltation and suspension as transport modes, comparable to natural sediment. The results show a strong correlation between the transport stage and the percentage of time in which microplastics experienced a certain mode of transport. Based on the laboratory results, a new phase diagram for microplastics is introduced, analogous to an existing diagram for sediments.

## 1. Introduction

Microplastics are abundant in aquatic environments, posing a pervasive environmental concern (Browne et al., 2011; Koelmans et al., 2019; Rhodes, 2018; Sundt et al., 2015). In response, various initiatives, spanning legislative, scientific, and social realms, target reduced microplastic emissions and the removal of environmental microplastics (Barcelo and Pico, 2020; Nikiema et al., 2020). The success and advancement of these initiatives are impeded by our limited ability to assess and monitor their performance and outcomes (Whitehead et al., 2021). A comprehensive understanding of microplastic transport pathways, such as the vertical distribution in the water column, is crucial for accurately estimating quantities, advancing risk characterization by comparing established effect thresholds with these estimated quantities, and evaluating the efficacy of removal initiatives. Especially the mechanisms governing microplastic transport in rivers, which represent an important route for microplastics to the oceans (Klein et al., 2015; Lebreton et al., 2017; Lechner et al., 2014; Rech et al., 2014), remain not fully understood (Waldschläger et al., 2022).

Flow characteristics can influence the transport of microplastic particles in rivers in a manner comparable to other natural riverine components (e.g., sediment, organic matter and air bubbles) (Cowger et al., 2021; Lofty et al., 2023; Waldschläger and Schüttrumpf, 2019a). Recently, the literature on microplastics has been enriched by efforts examining the applicability of the fundamental principles governing the flow-sediment interactions and the resulting modes of transport to fill this knowledge gap. Examples include the settling and rising velocity of microplastics based on equations known for sediment (Van Melkebeke et al., 2020; Waldschläger and Schüttrumpf, 2019a), the estimation of the vertical distribution of microplastics in the water column using the Rouse model (Born et al., 2023; Cowger et al., 2021; Eggenhuisen et al., 2020), the incipient motion of microplastics based on the Shields number (Waldschläger and Schüttrumpf, 2019b), and the saltation behaviour of spherical microplastics compared to sediments (Lofty et al., 2023).

Microplastics were found to be transported in suspension and as bed load, analogous to natural sediment (Born et al., 2023). However, the broad variation in density and particle geometry challenges the direct adoption of equations and models developed for sediment transport. For instance, the settling velocity and the critical shear velocity dictating the incipient motion of microplastics varied largely from the theoretical values based on sediment transport equations (Waldschläger and Schüttrumpf, 2019b, 2019a). Our understanding of the modes of transport experienced by microplastic particles (i.e., suspension or bed load) has benefited from recent work in the field. For instance, the work of Lofty et al. (2023) showed that the probability of saltation and rolling was governed by the Rouse number at the particle scale for perfect spheres with size and density ranges comparable to microplastics. Here, we further investigate the modes of transport of microplastic particles with different shapes, including fibres, fragments, pellets and spheres, under different turbulent flow conditions. Guided by the well-established practice in natural sediment (Abbott and Francis, 1977; Francis, 1973; Nino et al., 2003), we focus on the transport stage, referring to the ratio between the flow shear velocity ($U_*$) and the particle settling velocity ($W_s$), as a key parameter in describing the trajectory and transport modes exhibited by microplastics.

Our primary objectives are to establish and understand particle trajectories, encompassing the mean position in the water column ($Z_P$) and transport rate of plastic particles ($U_p$) with the flow. Based on further analysis of the particle trajectories we identify the different modes of transport encountered by microplastics, aiming to contribute essential insights for developing effective mitigation measures and predicting transport rates in river environments. Informed by our laboratory experiments, we provide the first phase diagram to predict microplastics modes of transport based on the transport stage.

## 2. Material and methods

### 2.1. Material matrix

A total of 24 types of microplastics were examined in the present study (Figure 1). The selection of microplastics was based on the types of polymers and shapes predominantly found in riverine systems (Duis and Coors, 2016; Kumar et al., 2021a; Mai et al., 2020). The particles cover a density range between 1.04 and 1.49 g cm $^{-3}$, and the upper limit of the nominal particle diameters was approximately 5 mm, which is the commonly used upper size limit for microplastics (NOAA, 2008). The lower limit was approximately 0.5 mm as it is the smallest size detectable by the cameras adopted for the experimental set-up. Further, the selected microplastics included a variety of shapes including spheres, semi-spheres (balls), fibres, fragments, cylinders, and lentils. The microplastic particles were coated with a thin layer of water-based black ink, serving dual purposes. Firstly, this coating minimized the influence of surface roughness and variations in affinity to air bubbles and water among different polymers, factors deemed beyond the study's scope. Secondly, it enhanced the visibility of the particles for the tracking system, ensuring accurate and effective monitoring. To account for the diversity and complexity of the particle shapes, dimensionless shape descriptors proposed by Van Melkebeke et al. (2020) were used. The shape factors used in the present study are summarized in Table 1.

Table 1: Summary of the descriptive shape factors adopted for the present study.

| Shape factors | | | | | |
|---|---|---|---|---|---|
| Corey shape factor ($CSF$) | Sphericity ($\phi$) | Elongation ($e$) | Flatness (F) | Aspect ratio ($\varphi$) | Nominal diameter ($d_n$) |
| $\frac{S}{\sqrt{LI}}$ | $\frac{A_{sph}}{A_p}$ | $\frac{I}{L}$ | $\frac{S}{I}$ | $\frac{I+S}{2L}$ | $\sqrt[3]{L \times I \times S}$ |
| **Input parameters** | | | | | |
| L (mm): orthogonal long axis | | $d_p$ (mm): the diameter of an equivalent sphere ($\sqrt[3]{\frac{6}{\Pi} v_p}$) | | | |
| I (mm): intermediate axis | | where $v_p$ (mm³): the measured volume of the particle | | | |
| S (mm): short axis | | | | | |
| $A_{sph}$ (mm²): the surface area of the equivalent sphere $4\pi\left(\frac{d_p}{2}\right)^2$ | | | | | |
| $A_p$ (mm²): the surface area of the particle, which is calculated as $2\pi rh + 2\pi r^2$ for perfect cylinders and as $\left(4\pi\left[\frac{\left(\frac{L}{2}\right)^2\left(\frac{I}{2}\right)^2+\left(\frac{L}{2}\right)^2\left(\frac{S}{2}\right)^2+\left(\frac{I}{2}\right)^2\left(\frac{S}{2}\right)^2}{3}\right]^{1/2}\right)$ for the remaining particles | | | | | |

The classification of the particles included two steps. First, the three principal dimensions $L$, $I$, and $S$ were determined for each particle primarily using Image J (see Table 1). A caliper was used to determine the third dimension whenever the particle geometry did not allow for adjusting the orientation of the particles in the images to determine the third dimension. In both cases, these three dimensions were determined based on the average of 10 measurements per microplastic type, following the work of Kerpen et al. (2020). The percentage standard deviation was reported for the three principal dimensions ($\mathrm{STD\%} = 100 \cdot \frac{\mathrm{STD}}{\overline{\mathrm{X}}}$, where $\overline{\mathrm{X}}$ is the mean of the measurements of the dimension of interest). The three principal dimensions were used to calculate the aspect ratio ($\varphi$), Corey shape factor ($CSF$), flatness (F), and elongation ($e$). Further, the settling velocities of the particles were calculated following the equation developed by Waldschläger & Schüttrumpf (2019a). This method in determining the settling velocity was based on the availability of information about the particle shape and its proven reliability compared to other methods (Van Melkebeke et al., 2020) for the range of particles used in the present study. Therefore, the nominal particle diameter was determined ($d_n$) using the equation in Table 1, which was the input parameter for the settling velocity calculations. Additionally, the particle density and size were characterized using the dimensionless particle diameter, $D_*$, defined as

$$D^* = \left(\frac{Sg}{v}\right)^{\frac{1}{3}} d_n$$

, where ν is the kinematic viscosity of the fluid (m²/s) and S is the ratio of excess particle density to water density (-), defined as

$$S = \frac{\rho_{particle} - \rho_{water}}{\rho_{water}}$$

This parameter is used both in sediment and in microplastic analyses (Camenen, 2007; Dietrich, 1982; Waldschläger and Schüttrumpf, 2019a; Zhiyao et al., 2008).

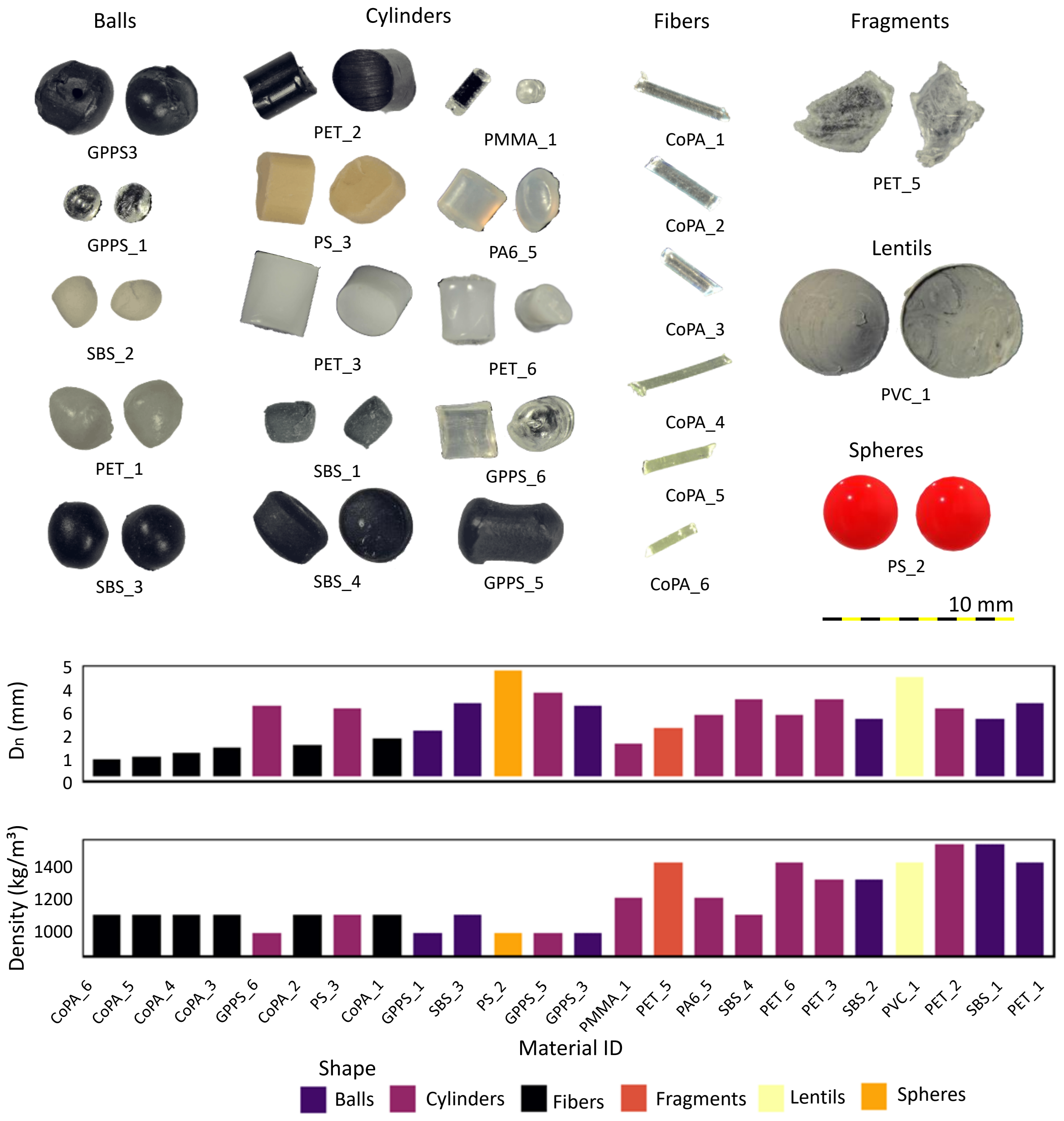


Figure 1: an overview of the tested microplastic particles properties (further information on the corresponding shape factors can be found in supplementary materials).

## 2.2. Experimental setup

A 5 m long recirculating flume with a cross-section of 450 mm by 300 mm at the Kraijenhoff van de Leur Laboratory at Wageningen University was used for the experiments. The flume allows for a maximum discharge of 40 l $s^{-1}$ with an adjustable slope (Figure 2) and the water depth can be controlled through a vertical gate downstream of the flume. The experiments were conducted using a fixed flume bed, where a layer of fine sand (with a diameter of 1.85 mm) was glued to the bed to introduce a roughness sufficient to establish fully developed turbulence conditions. The transport of each microplastic group was assessed under three flow conditions (Table 2). The selected flows represented subcritical turbulent flow conditions. The flow conditions were not scaled to a specific river, rather they were selected based on flows commonly occurring in natural rivers. The flow velocity profiles in two dimensions (parallel to the flow (u), and orthogonal to the flume bed (w)) were obtained at the centreline of the effective section using a UB-Lab 2C velocity vector profiler (ADVP). Instantaneous velocity measurements were used to obtain the bed shear velocity.

Table 2: Overview of flow conditions within the experimental setup.

| Flow condition | Discharge | Water depth | Mean velocity | Reynolds number | Froude number | Shear velocity | Bed slope |
|---|---|---|---|---|---|---|---|
| ID | Q | H | U | Re | F | $U_*$ | S |
| (-) | ($m^3/s$) | (cm) | (m/s) | (-) | (-) | (m/s) | (-) |
| F1 | 40.0 | 17.4 | 0.83 | 14442 | 0.635 | 0.103 | 0.15% |
| F2 | 25.0 | 23.0 | 0.47 | 10810 | 0.313 | 0.051 | 0.15% |
| F3 | 15.0 | 24.3 | 0.31 | 7533 | 0.201 | 0.018 | 0.15% |

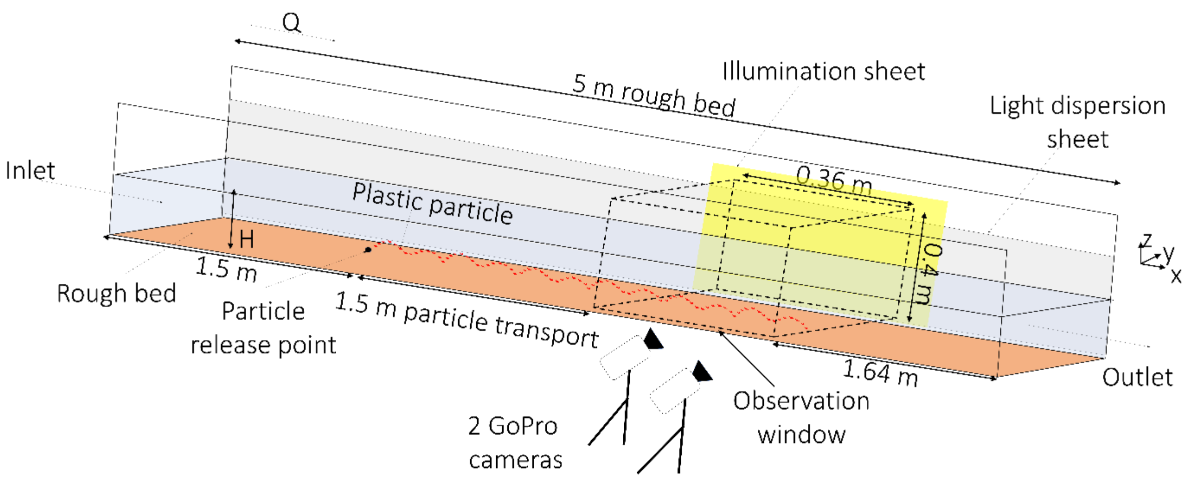


Figure 2: Layout of the experimental setup (distances not to scale).

### 2.3. Loading regime

The microplastics were introduced 1.5 m from the flume inlet, specifically at the centreline of the flume bed, given the density range of the tested microplastics (>1 g/cm³). To minimise the interference with the flow, a 3 cm wide and 30 cm long stainless-steel clamp was used to place the particle on the flume bed. This positioning aimed to initiate particle motion from their terminal position relative to settling velocities. The particles were transported freely for 1.5 m before reaching the observation window, where their transport trajectory was recorded. This approach ensured that the particles attained equilibrium before tracking their transport and minimized the influence of the flume inlet and outlet, located 3 m and 1.64 m away from the observation window, respectively. Additionally, prior to injection into the flume, the particles underwent water soaking to prevent air bubbles from attaching to their surfaces.

### 2.4. Particle tracking setup and analysis

The motion and transport of the microplastic particles were recorded using a particle tracking photogrammetry setup (PTV). The setup was composed of two GoPro Hero 11 cameras, which allowed for collecting videos with a frame rate of 50 fps and 5.3 K resolution. The cameras were located facing one side of the flume wall, covering an observation window of 0.36 m parallel to the flow direction (5312 pixels) and about 0.3 m perpendicular to the flow direction (2933 pixels). To improve the contrast between the tracked particles and the background, the roughened flume bed was sprayed with a thin layer of white paint. Further, a light source was placed facing the cameras on the other side of the flume where a dispersive white sheet was used to evenly distribute the light. The use of two synchronized cameras allowed for generating the 3D trajectory of the particles, by employing the concepts of epipolar distance and stereoscopy (Willneff, 2003). Although both cameras were controlled using a remote control to start recording at the same starting point, further postprocessing was needed to ensure that frames obtained from both cameras were in synchronization. This was achieved through postprocessing based on a distinctive sound at the beginning of the video recording. The calibration for the cameras was performed using a 3D calibration grid placed in the observation window at a known distance relative to the flume coordinate system.

The trajectory of the particles was obtained using stereoscopic reconstruction following the work of Douxchamps et al. (2005). The collected videos were treated using a MATLAB code developed in-house, where first the video frames were obtained, and then transformed from RGB to grayscale. Further, foreground detection was performed to separate the particles from the background and determine their centroid in each frame relative to the camera 2D coordinate system. For some frames, noise elimination was achieved by cropping the frame to the segment of interest where the particle is moving. Then, translation for the camera 2D coordinates system to real-world 3D coordinates was performed with the aid of the camera translation vector and rotation matrix obtained from the calibrations. The calibration and retrieval of the 3D trajectories was performed following the work of Spinewine et al. (2003). The detection of the 3D trajectories did not account for refraction. However, the camera angles were kept very low relative to the flume glass walls, to limit the effect of refraction (Kwon and Casebolt, 2006). The system accuracy was determined based on its capacity to detect multiple predefined reference points of known coordinates at different locations within the observation window. The developed setup allowed for the reconstruction of the reference points coordinates with an accuracy of ± 5 mm, which is sufficient for the present study objectives.

A total of 720 individual runs were conducted, including 24 microplastic particles under 3 different flow conditions, with 10 repetitions each. The selection of this number of test repetitions aligns with established practices in literature (Lofty et al., 2023; Waldschläger and Schüttrumpf, 2019b). The experimental assessment involved instantaneous measurements systematically organized based on flow and material variables, where each measurement of velocity and position represented a statistically independent event. To evaluate test reproducibility, the relative error was determined for both mean particle position and mean forward velocity for each flow-particle combination. In the context of classical sediment studies, the analysis of particle transport trajectories traditionally focuses on suspended sediments (Francis, 1973; Niño and García, 1998). In the present study we adopt a similar approach in defining the mean forward velocity and position of the particle. The mean forward velocity ($U_p$) is the average particle velocity component parallel to the primary flow direction (u), calculated as the average of all recorded instantaneous velocities. Similarly, the mean position in the water column ($Z_p$) is the average particle position within the water column relative to the flume bed, measured as the average of the recorded instantaneous particle positions. This approach allows for predicting microplastics transport and occurrence relative to the water column regardless of their modes of transport, with an acceptable accuracy of about ±25%. This is in line with the range of variation in particle velocity between the different modes of transport as shown by Frances (1973) for sediments.

The study focuses on three transport modes: rolling/sliding, saltation, and suspension, mirroring key modes identified in sedimentology (Abbott and Francis, 1977; Francis, 1973). The individual modes were determined based on analysing the full particle trajectory following predefined criteria (Figure 3). If all measurement points between two points of contact with the bed were below the longest particle dimension (a), the particle was classified as rolling/sliding. Trajectories without local minima but with one or more local maxima were categorized as saltation, and in cases where both local maxima and minima occurred, the particles were considered to be in suspension. Then, the full trajectory was segmented into intervals corresponding to each transport mode. These segments were translated into a percentage of time relative to the total duration it took for the particle to pass through the observation window. To streamline this process, a MATLAB code was developed for accurate and efficient analysis. While this approach effectively addressed spherical and semi-spherical particles, additional visual inspection became imperative for other particle shapes. This need arose because multiple additional local maxima and minima were encountered in trajectories due to the rotation of particles and changes in the dimension facing toward the cameras. Thus, visual inspection was necessary to filter out these observations as they are irrelevant to the modes of transport. Moreover, this step proved crucial for rectifying errors in estimating particle locations due to inaccuracies caused by the physical limitations of the setup.

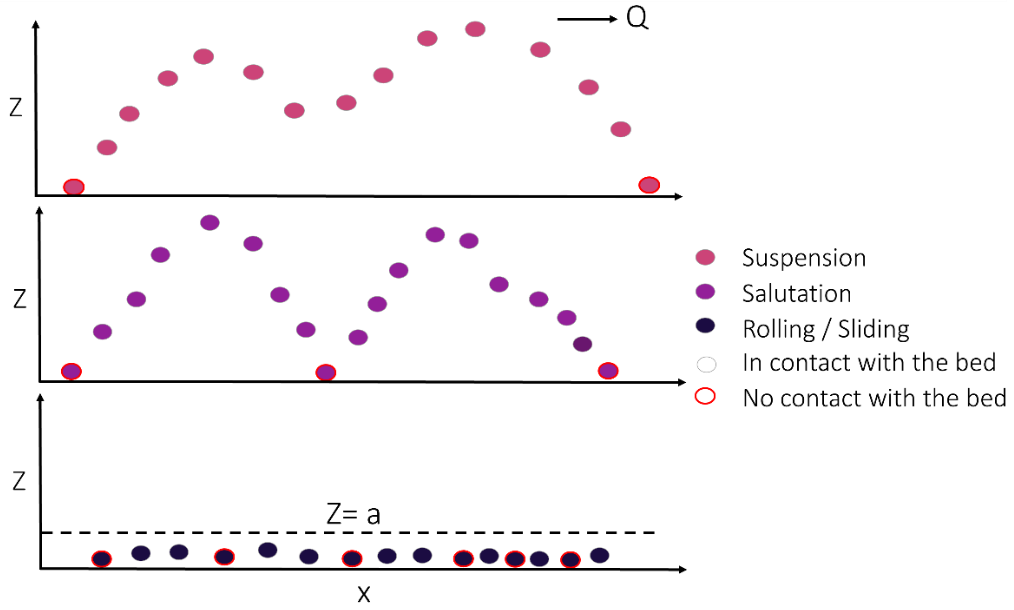


Figure 3: Conceptual diagram illustrating the criteria for determining the particle modes of transport.

Following the video analysis process, the impact of particle characteristics on the particle trajectory was examined through principal component analysis (PCA) and a multi-variable Anova test. The PCA test was utilized to determine the overall structure and patterns in the data, and to determine the variables describing most of the variances in the data. Then, the Anova test provided information about the statistical significance of each variable. Combining PCA and the Anova test results allowed for a comprehensive understanding of the underlying structure and the key variables governing the variations in the dataset. The tests were performed using R studio and the detailed results can be found in the Supplementary Material. The particle shape was evaluated using the five descriptive shape factors introduced earlier, while $D_*$ was used to examine the combined effect of size and density.

## 3. Results and discussion

The findings of the present study are outlined in two subsections. In the particle trajectory section, results regarding the mean forward velocity and mean particle position are presented, focussing mainly on the test reproducibility, the impact of the transport stage and the effect of the particle characteristics. In the next section, the impact of the particle characteristics and the transport stage on the modes of transport are presented.

## 3.1. Particle trajectory

### 3.1.1. Test reproducibility and reliability

Test reproducibility was assessed through the calculation of the relative error, considering all instantaneous measurements for each flow-particle combination. This comprehensive analysis provided a robust evaluation of the reliability of the experimental results across various conditions. In Figure 4, the resulting relative errors are graphically depicted in an ascending order based on the dimensionless particle diameter ($D_*$). The relative error concerning mean particle position exhibited a range from 0.5% to 7.4%. There was an observable trend of decreasing relative error with increasing particle density, suggesting a potential restriction in the randomness of the process for denser particles that tend to remain closer to the bed. Conversely, the relative error increased as the flow increased, which could be attributed to increased scatter introduced by higher turbulence. Lower relative errors were apparent in the mean forward velocity, ranging between 0.61% and 3.05%. Overall, an increase in particle density was associated with an increase in relative error for the mean forward velocity, indicating a higher level of randomness introduced by the friction forces impeding the particle transport due to increased particle-bed interactions.

Further, fragmented PET particles (PET_5) had one of the highest relative errors for the position (up to 6.5%), which could be attributed to the variabilities in the fragment shapes as they are the most heterogeneous particles in the present study. Indeed, the three principal dimensions determined for fragmented PET had the highest percentage standard deviation, ranging between 40 and 80%. This observation supports the assumption that shape and size are crucial factors in determining microplastics occurrence and transport in the water column.

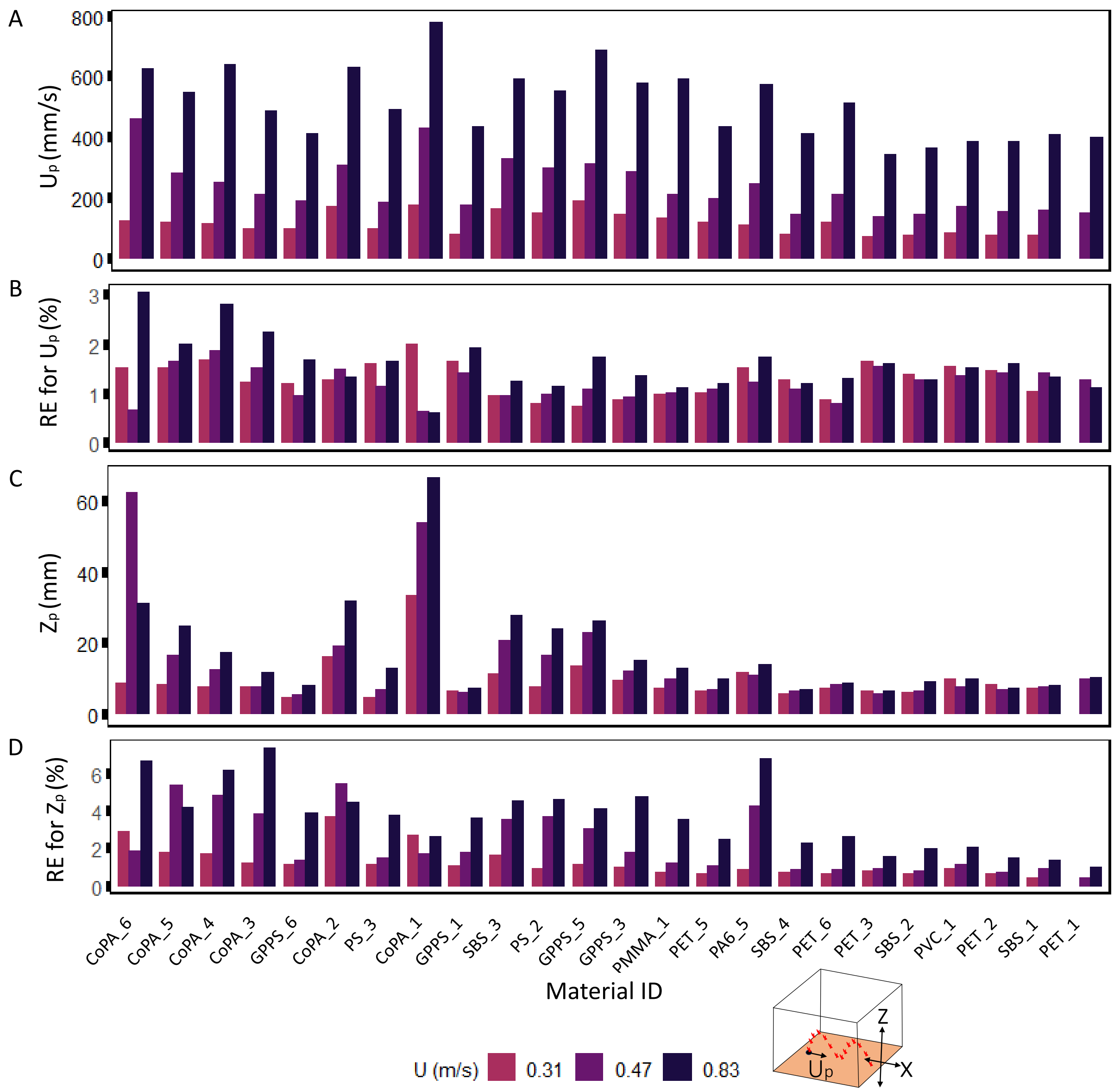


Figure 4: Mean results of the experiments grouped by material type and ordered by $D_*$ in an ascending order. A) The mean forward velocity. B) The relative error of the mean forward velocity, C) The mean particle position in the water column ($Z_P$), D) The relative error for $Z_P$. The specific characterestics of the particle are presented in Figure 1.

### 3.1.2. The impact of turbulence - Trajectory correlation with the transport stage

In previous studies, focusing on both sediments and microplastics, the normalized particle trajectory characteristics were found to be dependent on the transport stage ($U_*/W_s$), representing the ratio between bed shear and the particle settling velocities (Abbott and Francis, 1977; Francis, 1973; Lofty et al., 2023; Nino et al., 2003; Niño and García, 1998). In the present study, despite one anomaly discarded for the smallest fibre (CoPA_6), the particle mean velocity normalized to the flow velocity (U) and position normalized to the equivalent particle diameter ($D_{eq}$), were strongly correlated with the transport stage, which was found to be a statistically significant factor ($p$ value < 0.05) based on the Anova test. Higher stage ratios correspond to scenarios with increased relative turbulent forces, influencing the trajectory characteristics. Figure 5 illustrates the strong correlation between the normalized particle trajectory characteristics and the transport stage, fitting well to a power function. These results confirm the suitability of the power function proposed by Lofty et al. (2023) for the saltation trajectory characteristics of spheres, to the mean forward velocity and particle position introduced in the present study, albeit with lower correlation values. The lower correlation could be attributed to the fact that the mean forward velocity and position here represent a heterogeneous mix of particle transport regimes, combining saltation, suspension and rolling. For the present study, the particle position was normalized to $D_{eq}$, whereas in previous work on spheres the diameter of the particle was used for normalization (Abbott and Francis, 1977; Lofty et al., 2023). Such an approximation of the particle length scale could reduce the correlation for the mean normalized particle position ($Z_p$/ $D_{eq}$). The forces governing particle transport in the flow are strongly correlated with the surface area (Waldschläger and Schüttrumpf, 2019b). As the particles deviated from perfect spheres, the fluctuations in the surface area of a rotating particle perpendicular to the flow increased. As a result, the variations in the forces balance increased leading to a lower correlation. Further, the drag coefficient and settling velocity of the particles were determined based on equations developed for settling column experiments. The deviation from spherical particles in the present study produces complex relations between the flow condition and the drag coefficient which can largely affect the transport and settling processes of microplastics (Holjević et al., 2023). Further investigation of the drag coefficient and settling velocity in turbulent flow streams can contribute to better determination of particle behaviour and transport.

The results indicated a positive correlation between the particle location ($Z_P$) relative to the water depth (H) and the normalized mean forward velocity ($U_p$/U). Under the same flow conditions, particles present closer to the water surface experienced higher velocities. These findings align with the work of Francis & Abbott (1977), where an increase in water depth resulted in higher forward velocities of saltating particles. The position of the particle relative to the water column can lead to the particle being at different heights within the logarithmic velocity profile which explains the positive correlation between the particle forward velocity and particle position ($R^2$ = 0.65). In terms of particle position, the water depth was found insignificant in the present study, which deviated from the observations in the work of Francis & Abbott (1977). The water depth in the present study allowed the particles to reach maximum height without rebounding from the surface, which could explain the discrepancy.

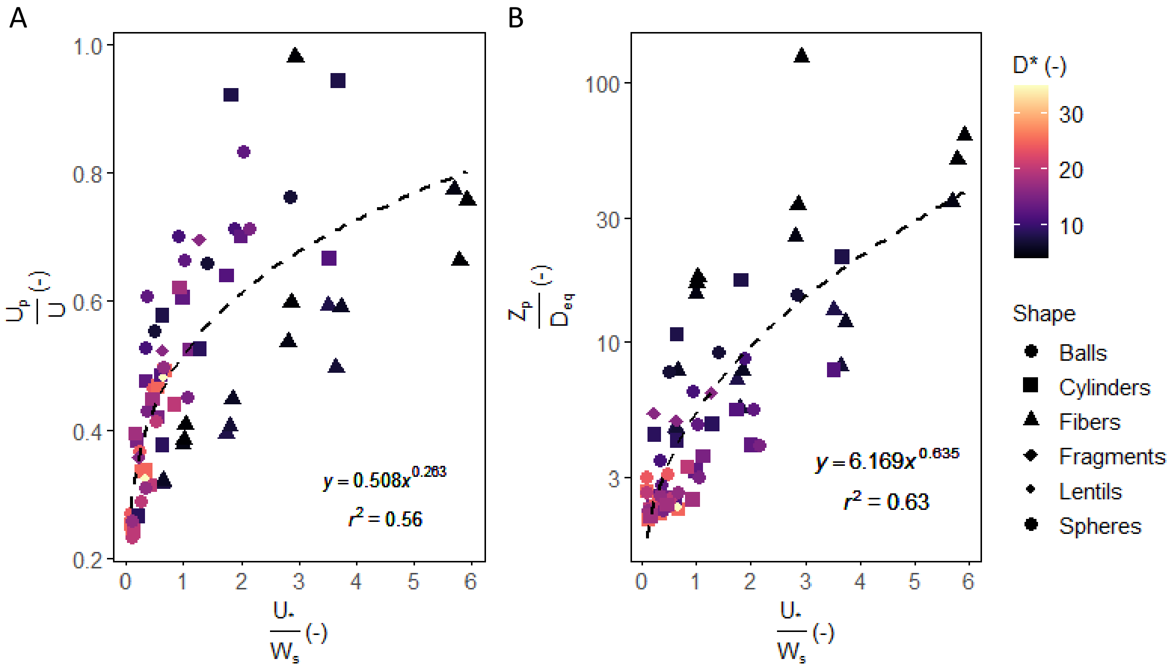


Figure 5: A) The mean forward velocity of the particles relative to the transport stage and B) the mean particle position relative to the transport stage. It is important to note that, for $Z_P$, an anomaly was

observed in the mean position of the smallest PA fibre (CoPA_6), necessitating its exclusion from the fit.

### 3.1.3. The impact of particle characteristics on particle trajectory

Employing PCA statistical tests indicated that CSF, elongation, sphericity, and aspect ratio play pivotal roles in the normalized particle velocity and position. The PCA test shows that these four shape factors can be interpreted collectively to explain up to 55% of the variance. The second principal component of the PCA is primarily affected by the transport stage and $D_*$. Utilizing a significance threshold of $p < 0.05$, the Anova test highlighted that elongation is the significant contributor for the normalized mean position. In terms of normalized mean forward velocity, significant contributors included elongation and aspect ratio. This variation in the results between PCA and the Anova implies a redundancy or overlap between the information conveyed by the different shape factors. This overlap could be explained by the fact that the shape factors are strongly correlated among each other as they are all derived from the particle side lengths. For both the normalized mean position and forward velocity, $D_*$ and the transport stage are significant contributors. The results are illustrated in Figure S4 and Tables S1 & S2 within the supplementary materials.

Despite their statistical significance, the shape factors maintained relatively low regression values individually ($r^2$ ranged between 0.005 and 0.35), compared to the transport stage. However, the impact of particle properties can be observed qualitatively in Figure S2, showing a scatter of the normalized mean forward velocity and mean position against the transport stage, where the impact of the particle properties is visualised. The particle normalized position and mean forward velocity decreased as $D_*$ decreased, similar to the observations for sediments (Francis, 1973). Relying only on $D_*$ proves insufficient in explaining the overall trend. In addition to gravitational forces, two crucial forces, buoyancy and drag, can act on a particle moving in water. These forces are intricately linked to the particle's surface area, which, in turn, is influenced by its geometry (Waldschläger and Schüttrumpf, 2019b). Notably, fibres exhibit a higher susceptibility to suspension in the water column compared to fragments and spherical particles, due to their increased buoyancy and reduced settling velocity (Kumar et al., 2021b). In our study, fibres reached the highest normalized mean position in the water column (Fig 4). This observation aligns with an inverse correlation between the normalized mean particle position and sphericity and elongation. The lift force, influenced by the particle's surface area, tends to push the particle higher in the water column as it deviates from a perfect sphere.

In terms of the normalized mean forward velocity, fibres had lower velocities compared to spheres (Figure 5.A). This can be attributed to two key factors. Spherical particles are more prone to entrainment from the bed compared to fibres, where the particle entrainment potential is expected to increase as sphericity approaches one (Gomes and Mesquita, 2013; Waldschläger and Schüttrumpf, 2019b). Spherical particles experience less friction once in contact with the bed, leading to reduced kinetic energy loss during rolling or saltating. Moreover, the migration of non-spherical spheres is highly influenced by their orientation and rotation regime (Tohme et al., 2021). Fibres tended to exhibit an oscillating velocity, moving up and down, which could explain the large relative error for the mean forward velocity of fibres (Figure 4.B). Thereby, fibres needed more time to travel through the observation window, which reduced their average mean forward velocity.

## 3.2. Modes of transport - The phase diagram

In this study, all particles exhibited mobility, except for the PVC pellets with a shape similar to lentils (PVC_1), which remained stationary under the lowest flow condition. Unsurprisingly, the particle diameter ($D_*$) emerged as a determinantal factor for the three distinct transport modes exhibited by the particles based on both Anova and PCA tests (see Tables S1 & S2 and Figures S3 & S4). Higher $D_*$ values correlated with bedload transport, whereas decreasing $D_*$ values were associated with an increased duration of particle suspension. Further, the particle shape had a pronounced effect on the particle transport mode. Spherical particles exhibited susceptibility for rolling and saltation, while fibres demonstrated a proclivity for suspension. The PCA test showed that the particle shape factors CSF, sphericity, elongation, and aspect ratio where the primary contributors. The Anova test further confirmed the significance of the particle shape for the three modes of transport. Shape parameters, specifically elongation, manifested statistically significant influence on particle suspension behaviour. For bedload transport modes, encompassing saltation and rolling/sliding regimes, the particle shape factors CSF and elongation were found to be the statistically significant contributors. These findings highlighted the intricate interplay between particle geometry, surface area, and the governing forces influencing particle transport, hence aligns with previous observations in both sediment (Deal et al., 2023) and microplastic transport research (Waldschläger and Schüttrumpf, 2019b). For the saltation mode, the effect of the particle shape can play an additional role in the characteristics of the collision with the bed and the associated energy losses induced by the impact and the rebound dynamics (Ali SZ and Dey, 2019; Baran et al., 2018; Pähtz et al., 2020). Spherical particles have a constant projected area in contact with the bed at any collision point, which reduces heterogeneities in the collision and the associated energy losses. The contact area for other particles tends to vary over time, increasing the randomness of the collisions. Further investigation of the impact of the particle shape on the collision characteristics could prove influential in improving the predictability of microplastics saltation behaviour.

The modes of transport exhibited by the particles appeared to be correlated with the transport stage (see Figure S5 in supplementary materials). Due to the irregularly spaced nature of the collected data the fit was determined based on a locally weighted regression algorithm (LOESS) (Cleveland, 1979; Cleveland and Devlin, 1988). The analysis was performed following the method described in de Ruijsscher et al. (2018). It should be noted however, that the Anova test suggested that the transport stage is not a significant factor governing particle saltation, possibly due to the already discussed randomness of collisions for non-uniform particles (Table S2). While the normalization to the bed roughness has significantly improved the correlation for spherical particles in the previous work (Lofty et al., 2023), this impact was negligible in our investigation. This discrepancy can be attributed to the influence of particle shape, which profoundly alters the hiding exposure effect—a fundamental aspect addressed by the modified stage. For instance, fibres were found to be more prone to be trapped in the bed material compared to spherical particles (Waldschläger and Schüttrumpf, 2019a).

Previous sediment studies suggested that bed roughness becomes inconsequential for particle suspension when the ratio of particle diameter ($d_p$) to bed material diameter ($d_b$) exceeds 0.5 (Nino et al., 2003). This observation elucidates the insignificance of bed roughness in particle suspension in our study, given that all examined particles had a $d_p/d_b$ ratio greater than 0.5. Further examination of a wider range of bed material could contribute to unpacking the impact of the bed material on microplastics modes of transport.

Overall, the result of the present study allows for the generation of a phase diagram to predict the modes of transport experienced by a microplastic particle as a function of the transport stage (Figure 6). The obtained phase diagram is comparable to the transport diagram developed for sediment by Abbott & Francis (1977). In the present study, microplastics were found to be in motion at lower stage values compared to natural sediment, which could be explained by their lower critical shear as evident in the work of Waldschläger & Schüttrumpf (2019b). Further examination to improve the fit for the suspension phase can enhance the performance of the phase diagram as a prediction tool for the modes of transport of microplastic particles. It should be noted, however, that the presented phase diagram does not capture the full range of possible particle shapes at each stage value, due to the limited number of microplastic particles tested. For instance, at stage values above 3, fibres were the dominant particle shape, which could lead to a bias in predicting the modes of transport. Testing a wider range of shapes at each stage value could improve the phase diagram performance.

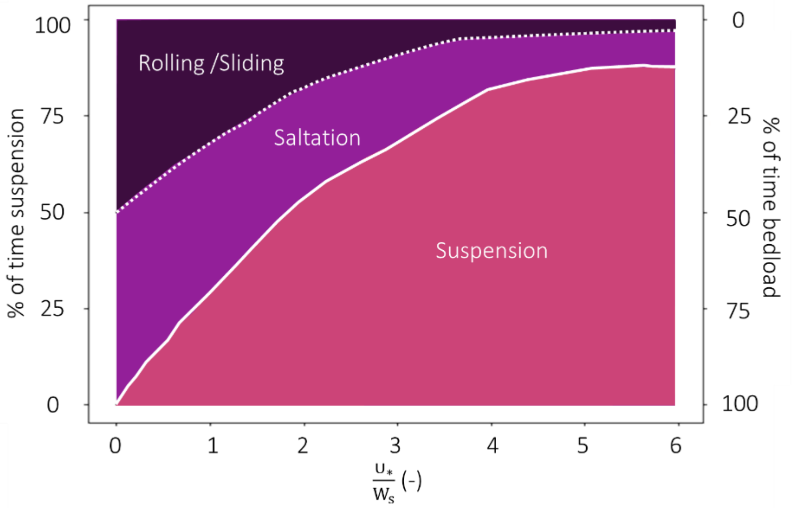


Figure 6: Phase diagram for the transport of microplastic particles, where the bedload covers saltation and rolling/siding

## 4. Conclusions

Flume experiments conducted in this study have yielded insights into the influence of particle shape, size, and density on the trajectory characteristics of microplastics across varying flow conditions. Utilizing a three-dimensional tracking system, we comprehensively analysed the trajectory of 24 types of microplastic particles with diverse characteristics. Our results revealed that the transport stage ($U_*/W_S$) can be used to effectively describe and predict the normalized mean forward velocity ($U_p/U$) and the normalized mean position in the water column relative to the bed ($Z_p/D_{eq}$), aligning with established practices in sediment studies. A correlation between the percentage of time a specific transport mode was encountered and the transport stage was found, enabling the development of a phase diagram for microplastics. Intuitively, the statistical analysis confirmed the dependence on the nominal particle diameter ($D_*$), describing density and nominal diameter, for the trajectory characteristics and modes of transport. Further, several particle shape factors emerged as primary determinant factors, indicating their pivotal role in governing particle behaviour.

In the present study, as particles deviate from a spherical shape, their susceptibility to suspension increased, accompanied by a decrease in their transport velocity). In terms of the mean position in the water column, fibres tended to be transported closer to the water surface compared to other particle shapes. However, the particle shape factors on their own displayed an overall week relation with the particle trajectory and transport mode. Once incorporated in the setting velocity calculations ($W_S$), and hereby also in the transport stage, they support a better understanding of the particle trajectories. These findings hold profound implications. Research suggests that fragments (particles of irregular shapes) represent the second most abundant microplastic shape in water and sediments (Burns and Boxall, 2018). Therefore, finding methods to describe their irregular shapes and to understand the shapes' impact on the transport dynamics of these microplastics becomes imperative. The particle shape plays a crucial role in determining the main coefficient dictating the forces governing particle transport in water (e.g., drag and friction coefficients). Further fundamental investigation of the impact of the particle shape on these forces could improve the predictability of their transport in riverine systems. Additionally, the diversity in particle shapes increases the complexity of the particle collision – a phenomenon inherent with particle saltation. Despite accounting for the particle shape in determining the transport stage in the present study, the particle saltation proved to be the least predictable. A deeper investigation of the collision characteristics for particles of different shapes could significantly improve the predictability of saltation behaviour for microplastics.

To enhance the robustness of our findings and refine the developed phase diagram, future research may explore a broader spectrum of bed materials and particle characteristics. Despite their pivotal significance, the comprehensive application of experimental investigations conducted at the particle scale, such as the present study, requires coupling with some descriptive models accounting for the full mixture of particle properties in the environment. Such coupling would undoubtedly contribute to a more comprehensive understanding of microplastics' complex behaviour in turbulent flows. Further, it can lead to a more robust mathematical integration of particle characteristics effects on transport models in the environmental domain.

In summary, this study underscores the parallels in behaviour between microplastics and sediments, emphasizing the role of particle characteristics (i.e., shape and $D_*$ which covers the size and density) in capturing potential differences. Our findings have significant implications for prediction models, providing valuable insights into transport rates and potential accumulation zones of microplastics in river systems. Utilizing the transport stage offers a simplified way to incorporate turbulence effects into transport models. The study results can be applied to predict the average transport rate and position of microplastics in rivers, supporting the development of targeted mitigation measures. Projecting the present findings regarding the effect of the particles shape on their distribution in the water column could support a better interpretation of sampling campaigns. In rivers, where turbulence is the dominant process governing plastic particle transport, fibres are more likely to be present at higher levels in the water column compared to spherical particles present closer to the bed. Hence, surface sampling is more likely to capture fibres while spheres are expected to be captured in sediment samples. Utilizing this knowledge when extrapolating microplastic particles abundance along the water column could support a better prediction of microplastics' abundance from single-point sampling measurements.

**CRediT authorship contribution statement**

Hadeel Al-zawaidah: Conceptualization, Methodology, Formal analysis, Investigation, Visualization, Writing – original draft, Writing – review & editing.

Merel Kooi: Supervision, and Writing – review & editing.

Ton Hoitink: Supervision, Funding acquisition, Formal analysis, and Writing – review & editing.

Bart Vermeulen: Conceptualization, Methodology, and Supervision.

Kryss Waldschläger: Conceptualization, Methodology, Supervision, Writing – review & editing.

**Declaration of Competing Interest**

The authors declare that they have no known competing financial interests or personal relationships that could have appeared to influence the work reported in this paper.

**Funding**

Hadeel Al-Zawaidah is funded by the Sectorplan Techniek 1, which aims to advance the technical sciences at Dutch universities. Bart Vermeulen is funded by the Sectorplan Techniek 1. The work of

Kryss Waldschläger was supported by the Veni Research Program, with project number 20084, which was (partly) financed by the Dutch Research Council (NWO).

## Acknowledgements

We would like to thank the lab team at the Kraijenhoff van de Leur Laboratory at Wageningen University, especially Nick Wallerstein and David Boelee, for facilitating and supporting the lab experiments and for designing the calibration object for the cameras. We would like to thank Iris Niesten, for the Matlab function to process the flow velocity profile data. For imaging the particles using the microscope we would like to thank Svenja Mintenig and Derk van Grootheest. Also, we would like to thank Svenja Fischer for her help with interpreting the statistical analysis and Roeland van de Vijsel for his feedback and thoughts on the data analysis method. Last but not least, we would like to thank Wei-Jay Ni from the University of Trento for his help with the code for the camera calibration.

## Data availability

Data will be made available on request.

## References

Abbott, J.E., Francis, J.R.D., 1977. Saltation and Suspension Trajectories of Solid Grains in a Water Stream. Philosophical Transactions of the Royal Society of London. Series A, Mathematical and Physical Sciences 284, 225–254.

Ali SZ, Z., Dey, S., 2019. Bed particle saltation in turbulent wall-shear flow: A review. Proceedings of the Royal Society A: Mathematical, Physical and Engineering Sciences. https://doi.org/10.1098/rspa.2018.0824

Baran, O., Eppinger, T., Kuanjin, H., 2018. DEM Simulation of Cylinders and Capsules in a Fluidized Bed, in: World Congress on Particle Technology. Orlando.

Barcelo, D., Pico, Y., 2020. Case studies of macro- and microplastics pollution in coastal waters and rivers: Is there a solution with new removal technologies and policy actions? Case Studies in Chemical and Environmental Engineering 2, 100019. https://doi.org/10.1016/j.cscee.2020.100019

Born, M.P., Brüll, C., Schaefer, D., Hillebrand, G., Schüttrumpf, H., 2023. Determination of Microplastics' Vertical Concentration Transport (Rouse) Profiles in Flumes. Environ Sci Technol 57, 5569–5579. https://doi.org/10.1021/acs.est.2c06885

Browne, M.A., Crump, P., Niven, S.J., Teuten, E., Tonkin, A., Galloway, T., Thompson, R., 2011. Accumulation of Microplastic on Shorelines Woldwide: Sources and Sinks. Environ Sci Technol 45, 9175–9179. https://doi.org/10.1021/es201811s

Camenen, B., 2007. Simple and General Formula for the Settling Velocity of Particles. Hydraul. Eng 133. https://doi.org/10.1061/ASCE0733-94292007133:2229

Cleveland, W.S., 1979. Robust locally weighted regression and smoothing scatterplots. J Am Stat Assoc 74, 829–836.

Cleveland, W.S., Devlin, S.J., 1988. Locally weighted regression: an approach to regression analysis by local fitting. J Am Stat Assoc 83, 596–610.

Cowger, W., Gray, A.B., Guilinger, J.J., Fong, B., Waldschläger, K., 2021. Concentration Depth Profiles of Microplastic Particles in River Flow and Implications for Surface Sampling. Environ Sci Technol 55, 6032–6041. https://doi.org/10.1021/acs.est.1c01768

de Ruijsscher, T. V., Hoitink, A.J.F., Dinnissen, S., Vermeulen, B., Hazenberg, P., 2018. Application of a Line Laser Scanner for Bed Form Tracking in a Laboratory Flume. Water Resour Res 54, 2078–2094. https://doi.org/10.1002/2017WR021646

Deal, E., Venditti, J.G., Benavides, S.J., Bradley, R., Zhang, Q., Kamrin, K., Perron, J.T., 2023. Grain shape effects in bed load sediment transport. Nature 613, 298–302. https://doi.org/10.1038/s41586-022-05564-6

Dietrich, W.E., 1982. Settling velocity of natural particles. Water Resour Res 18, 1615–1626. https://doi.org/10.1029/WR018i006p01615

Douxchamps, D., Devriendt, D., Capart, H., Craeye, C., MacQ, B., Zech, Y., 2005. Stereoscopic and velocimetric reconstructions of the free surface topography of antidune flows. Exp Fluids 39, 533–551. https://doi.org/10.1007/s00348-005-0983-7

Duis, K., Coors, A., 2016. Microplastics in the aquatic and terrestrial environment : sources ( with a specific focus on personal care products ), fate and effects. Environ Sci Eur 28, 1–25. https://doi.org/10.1186/s12302-015-0069-y

Eggenhuisen, J.T., Tilston, M.C., Leeuw, J., Pohl, F., Cartigny, M.J.B., 2020. Turbulent diffusion modelling of sediment in turbidity currents: An experimental validation of the Rouse approach. The Depositional Record 6, 203–216. https://doi.org/10.1002/dep2.86

Francis, J.R.D., 1973. Experiments on the Motion of Solitary Grains Along the Bed of a Water-Stream, Source: Proceedings of the Royal Society of London. Series A, Mathematical and Physical Sciences.

Gomes, L.M., Mesquita, A.L.A., 2013. Effect of particle size and sphericity on the pickup velocity in horizontal pneumatic conveying. Chem Eng Sci 104, 780–789. https://doi.org/10.1016/j.ces.2013.08.055

Holjević, T., Travaš, V., Družeta, S., Holjević, D., 2023. Experimental Assessment of Drag Coefficient for Quasi-Radially-Symmetric Microplastic Particles Sinking in Water Stream. J Mar Sci Eng 11. https://doi.org/10.3390/jmse11030549

Kerpen, N.B., Schlurmann, T., Schendel, A., Gundlach, J., Marquard, D., Hüpgen, M., 2020. Wave-Induced Distribution of Microplastic in the Surf Zone. Front Mar Sci 7. https://doi.org/10.3389/fmars.2020.590565

Klein, S., Worch, E., Knepper, T.P., 2015. Occurrence and Spatial Distribution of Microplastics in River Shore Sediments of the Rhine-Main Area in Germany. Environ Sci Technol 49, 6070–6. https://doi.org/10.1021/acs.est.5b00492

Koelmans, A.A., Mohamed Nor, N.H., Hermsen, E., Kooi, M., Mintenig, S.M., De France, J., 2019. Microplastics in freshwaters and drinking water: Critical review and assessment of data quality. Water Res 155, 410–422. https://doi.org/10.1016/j.watres.2019.02.054

Kumar, R., Sharma, P., Manna, C., Jain, M., 2021a. Abundance , interaction , ingestion , ecological concerns , and mitigation policies of microplastic pollution in riverine ecosystem : A review. Science of the Total Environment 782, 146695. https://doi.org/10.1016/j.scitotenv.2021.146695

Kumar, R., Sharma, P., Verma, A., Jha, P.K., Singh, P., Gupta, P.K., Chandra, R., Vara Prasad, P. V., 2021b. Effect of physical characteristics and hydrodynamic conditions on transport and deposition of microplastics in riverine ecosystem. Water (Switzerland). https://doi.org/10.3390/w13192710

Kwon, Y.H., Casebolt, J.B., 2006. Effects of light refraction on the accuracy of camera calibration and reconstruction in underwater motion analysis. Sports Biomech 5, 315–340. https://doi.org/10.1080/14763140608522881

Lebreton, L.C.M., Van Der Zwet, J., Damsteeg, J.W., Slat, B., Andrady, A., Reisser, J., 2017. River plastic emissions to the world’s oceans. Nat Commun 8, 1–10. https://doi.org/10.1038/ncomms15611

Lechner, A., Keckeis, H., Lumesberger-Loisl, F., Zens, B., Krusch, R., Tritthart, M., Glas, M., Schludermann, E., 2014. The Danube so colourful: A potpourri of plastic litter outnumbers fish larvae in Europe’s second largest river. Environmental Pollution 188, 177–181. https://doi.org/10.1016/j.envpol.2014.02.006

Lofty, J., Valero, D., Wilson, C.A.M.E., Franca, M.J., Ouro, P., 2023. Microplastic and natural sediment in bed load saltation: Material does not dictate the fate. Water Res 243, 120329. https://doi.org/10.1016/j.watres.2023.120329

Mai, L., Sun, X.-F., Xia, L.-L., Bao, L.-J., Liu, L.-Y., Zeng, E.Y., 2020. Global Riverine Plastic Outflows. Environ Sci Technol 54, 10049–10056. https://doi.org/10.1021/acs.est.0c02273

Nikiema, J., Mateo-Sagasta, J., Asiedu, Z., Saad, D., Lamizana, B., 2020. Water pollution by plastics and microplastics: a review of technical solutions from source to sea.

Niño, Y., García, M., 1998. Experiments on saltation of sand in water. Journal of Hydraulic Engineering, 124, 1014–1025.

Nino, Y., Lopez, F., Garcia, M., 2003. Threshold for particle entrainment into suspension. Sedimentology 50, 247–263. https://doi.org/10.1046/j.1365-3091.2003.00551.x

NOAA, 2008. Effects and Fate of Microplastic Marine Debris, in: Proceedings of the International Research Workshop on the Occurence.

Pähtz, T., Clark, A.H., Valyrakis, M., Durán, O., 2020. The Physics of Sediment Transport Initiation, Cessation, and Entrainment Across Aeolian and Fluvial Environments. Reviews of Geophysics. https://doi.org/10.1029/2019RG000679

Rech, S., Macaya-Caquilpán, V., Pantoja, J.F., Rivadeneira, M.M., Jofre Madariaga, D., Thiel, M., 2014. Rivers as a source of marine litter - A study from the SE Pacific. Mar Pollut Bull 82, 66–75. https://doi.org/10.1016/j.marpolbul.2014.03.019

Rhodes, C.J., 2018. Plastic Pollution and Potential Solutions. Sci Prog 101, 207–260. https://doi.org/10.3184/003685018X15294876706211

Spinewine, B., Capart, H., Larcher, M., Zech, Y., 2003. Three-dimensional Voronoï imaging methods for the measurement of near-wall particulate flows. Experiments in fluids 34, 227–241.

Sundt, P., Schulze, P.E., Syversen, F., 2015. Sources of Microplastic-pollution to the Marine Environment. Mepex for the Norwegian Environment Agency. Report no M-321.

Tohme, T., Magaud, P., Baldas, L., 2021. Transport of Non-Spherical Particles in Square Microchannel Flows: A Review. https://doi.org/10.3390/mi

Van Melkebeke, M., Janssen, C., De Meester, S., 2020. Characteristics and Sinking Behavior of Typical Microplastics including the Potential Effect of Biofouling: Implications for Remediation. Environ Sci Technol 54, 8668–8680. https://doi.org/10.1021/acs.est.9b07378

Waldschläger, K., Brückner, M.Z.M., Carney, B., Hackney, C.R., Adyel, T.M., Alimi, O., Belontz, S.L., Cowger, W., Gray, A., Kane, I., Kooi, M., Kramer, M., Lechthaler, S., Michie, L., Nordam, T., Pohl, F., Russell, C., Thit, A., Umar, W., Valero, D., Varrani, A., Warrier, A.K., Woodall, C.L., 2022. Learning from natural sediments to tackle microplastics challenges: A multidisciplinary perspective. Earth Sci Rev 104021. https://doi.org/10.1016/j.earscirev.2022.104021

Waldschläger, K., Schüttrumpf, H., 2019a. Effects of Particle Properties on the Settling and Rise Velocities of Microplastics in Freshwater under Laboratory Conditions. Environ Sci Technol 53, 1958–1966. https://doi.org/10.1021/acs.est.8b06794

Waldschläger, K., Schüttrumpf, H., 2019b. Erosion Behavior of Different Microplastic Particles in Comparison to Natural Sediments. Environ Sci Technol. https://doi.org/10.1021/acs.est.9b05394

Whitehead, P.G., Bussi, G., Hughes, J.M.R., Castro-Castellon, A.T., Norling, M.D., Jeffers, E.S., Rampley, C.P.N., Read, D.S., Horton, A.A., 2021. Modelling Microplastics in the River Thames: Sources, Sinks and Policy Implications. Water (Basel) 13, 861. https://doi.org/10.3390/w13060861

Willneff, J., 2003. A spatio–temporal matching algorithm for 3D Particle tracking velocimetry. PhD thesis. Siwss Federal Institute of Technology, Zurich.

Zhiyao, S., Tingting, W., Fumin, X., Ruijie, L., 2008. A simple formula for predicting settling velocity of sediment particles 1, 37–43.

Supporting information to:

# Mapping microplastic movement: A phase diagram to predict microplastics modes of transport

Hadeel Al-Zawaidah[1*], Merel Kooi[2], Ton Hoitink[1], Bart Vermeulen[1] & Kryss Waldschläger[1]

[1]: Wageningen University and Research, Hydrology and Environmental Hydraulics Group, Wageningen, The Netherlands

[2]: Wageningen University and Research, Aquatic Ecology and Water Quality Group, 6700 AA Wageningen, The Netherlands

[*]Email: hadeel.alzawaidah@wur.nl

Table of Contents

## S1) Material properties

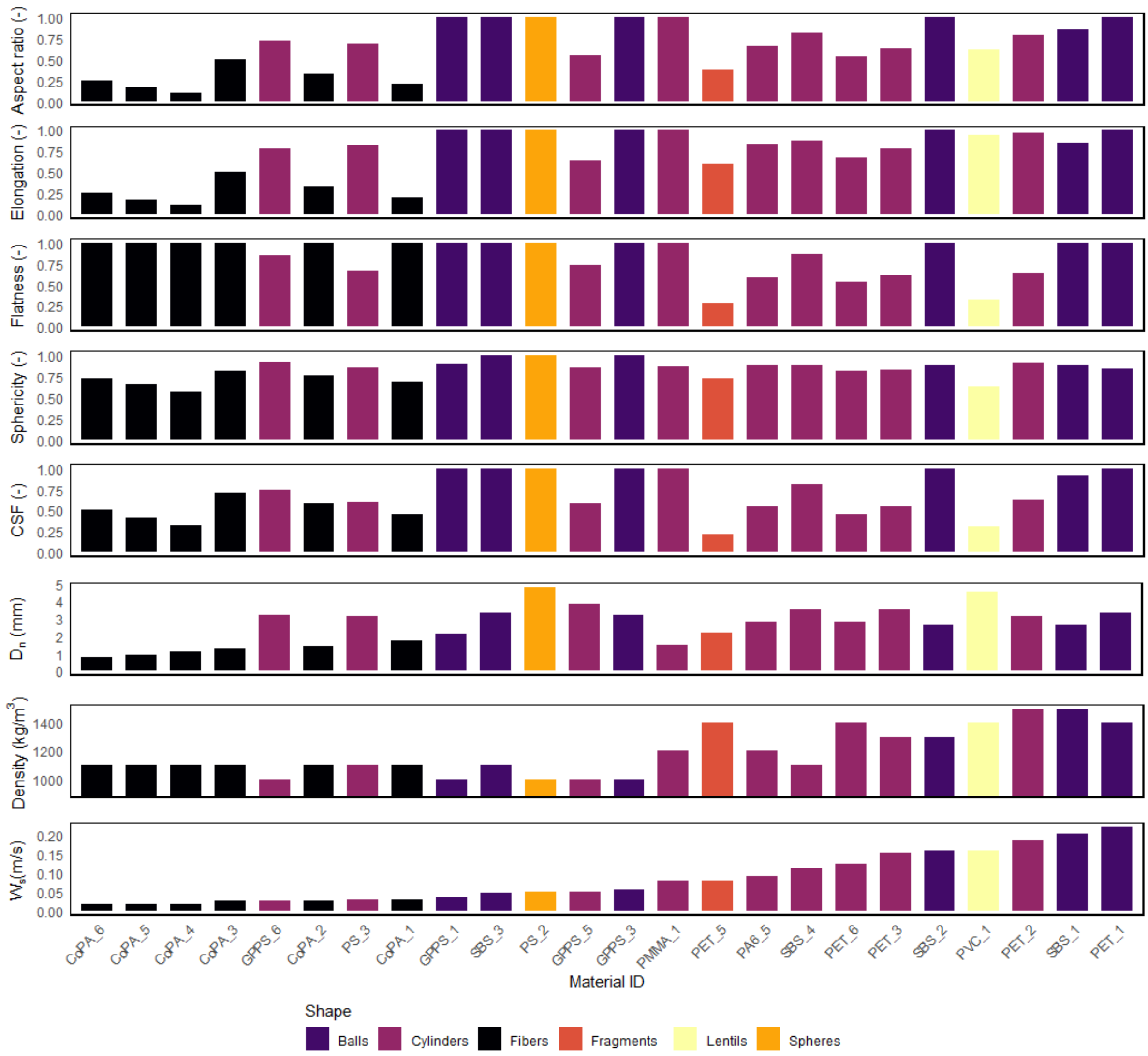


**Figure S1:** Layout of the particle properties.

## S2) Visual inspection of the effect of the particle shape

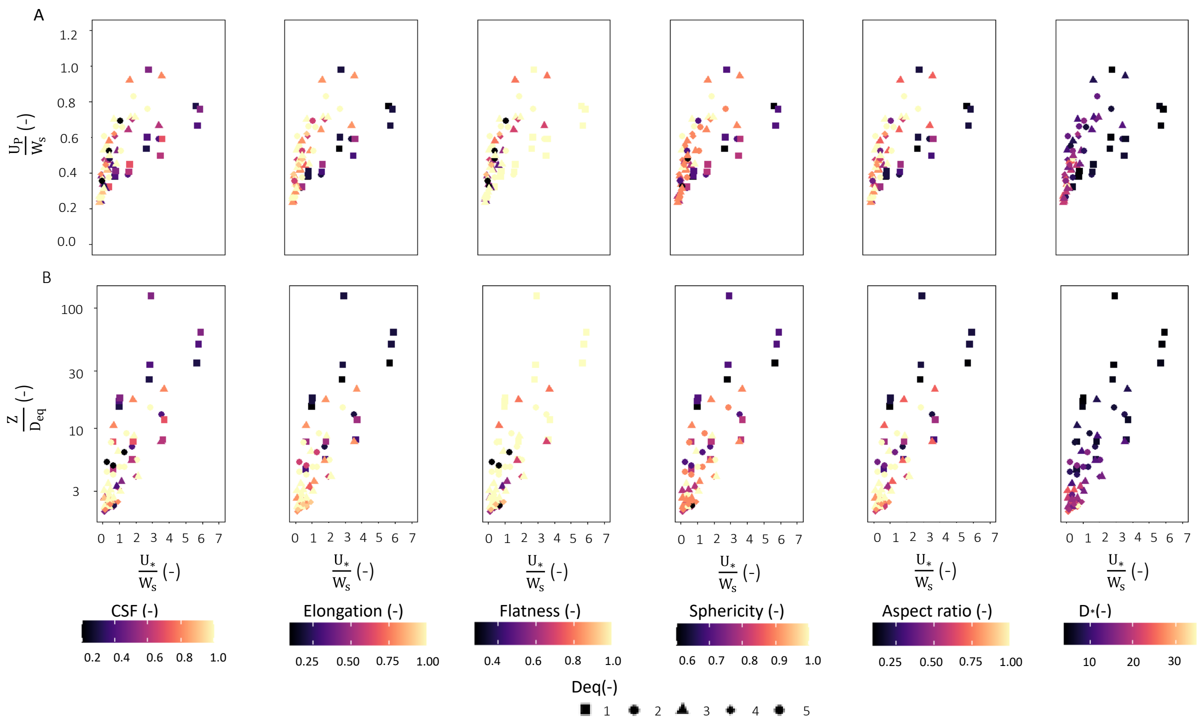


**Figure S2:** Layout of the particle trajectory characteristics faceted by microplastics characteristics.

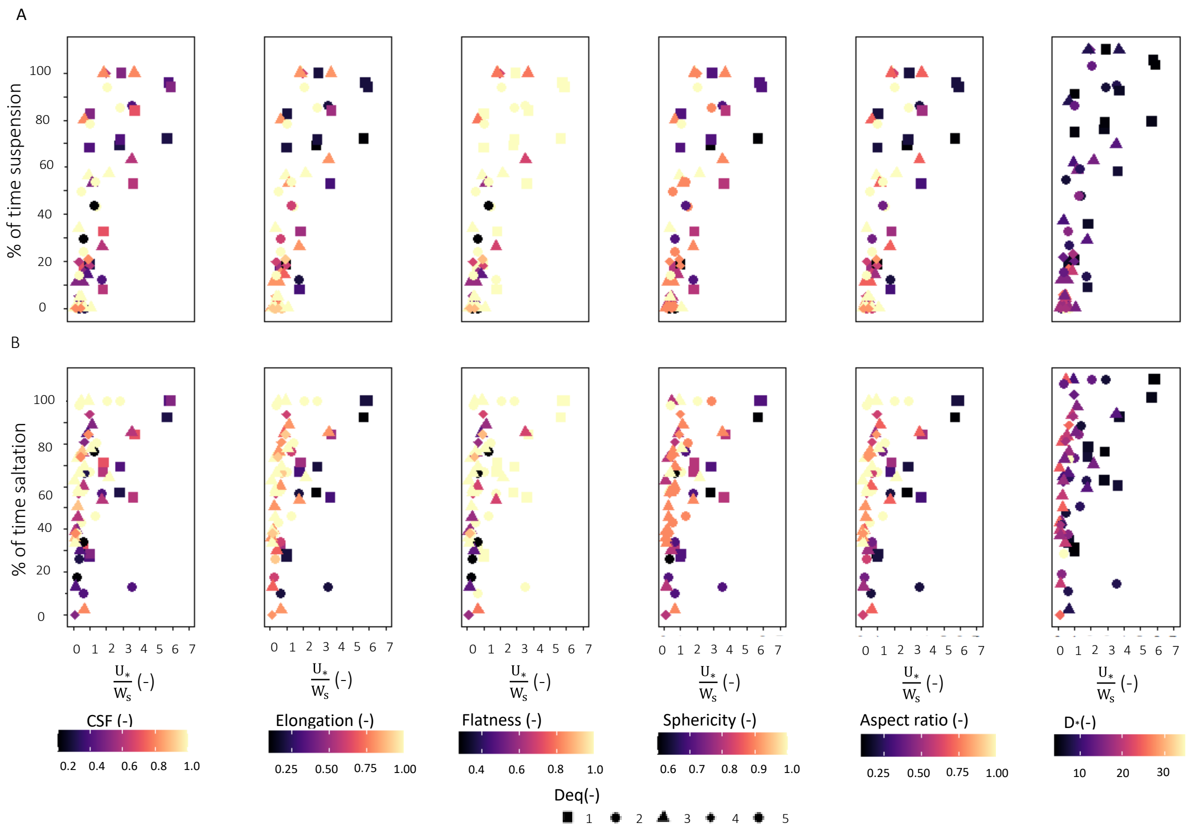


**Figure S3**: Layout of the particles modes of transport faceted by microplastics characteristics.

## S3) Statistical analysis of the effect of the particle shape

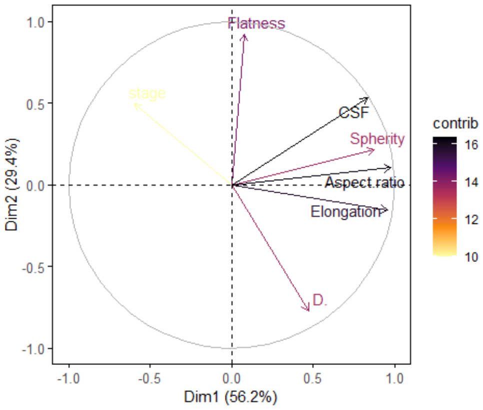


**Figure S4:** Graphical representation for the PCA results in the two primary principal components.

**Table S1 :** PCA loading results for the predictor variables.

| Parameter | PC1 | PC2 | PC3 |
|---|---|---|---|
| CSF | 0.42083961 | 0.37114203 | -0.08036899 |
| Sphericity | 0.44300254 | 0.15163019 | 0.23729534 |
| Elongation | 0.48419153 | -0.10847351 | 0.24345468 |
| Flatness | 0.03893025 | 0.64223866 | -0.39129138 |
| Aspect ratio | 0.49432135 | 0.07275268 | 0.13119666 |
| D* | 0.23813821 | -0.53861589 | 0.05266317 |
| $\frac{U_*}{W_S}$ | -0.29936994 | 0.34586826 | 0.83956337 |

**Table S2 :** Summary of the Anova test results.

| | P value | | | | |
|---|---|---|---|---|---|
| Parameter | $\frac{Z}{D_{eq}}$ | $\frac{U_P}{U}$ | % of time in suspension | % of time in saltation | % of time in rolling/sliding |
| CSF | 0.120909 | 0.607662 | 0.3883 | 0.00687 | 0.035184 |
| Sphericity | 0.073360 | 0.092176 | 0.4815 | 0.54678 | 0.857247 |
| Elongation | 0.001217 | 0.000346 | 9.55e-09 | 0.00185 | 0.000497 |
| Flatness | 0.411414 | 0.129317 | 0.0777 | 0.62975 | 0.132576 |
| Aspect ratio | 0.798507 | 0.048424 | 0.1643 | 0.82737 | 0.209002 |
| D* | 0.009648 | 4.23e-07 | 1.10e-07 | 0.00193 | 0.002448 |
| $\frac{U_*}{W_S}$ | 0.000849 | 8.65e-11 | 2.05e-08 | 0.16333 | 3.13e-07 |

**S4: Derivation of the phase diagram**

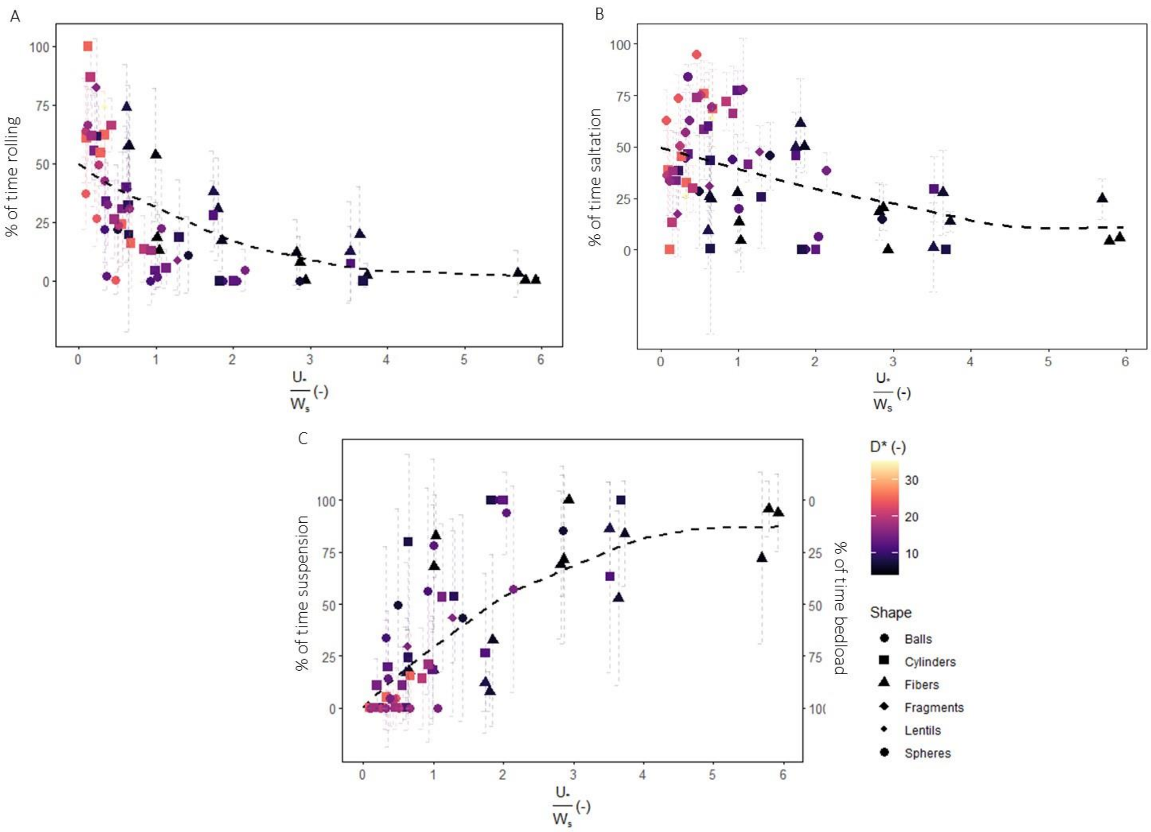


**Figure S5:** The percentage of time a particle exhibited rolling against the stage, A, the percentage of time a particle exhibited saltation against the stage, B, and the different modes of transport of the particles relative to the stage, C.